Ocean Engineering 340 (2025) 122354

Contents lists available at ScienceDirect

Ocean Engineering

journal homepage: www.elsevier.com/locate/oceaneng

Research paper

Sliding mode observer based non-causal model predictive control for collision-free marine launch and recovery system

Vincentius Versandy Wijaya [a], Yao Zhang [b,*], Christopher Edwards [c], Guang Li [d], Michael Belmont [c]

[a] School of Engineering, University of Southampton, Southampton, SO16 7QF, UK
[b] Department of Mechanical Engineering, University College London, London, WC1E 7JE, UK
[c] College of Engineering, Mathematics and Physical Sciences, University of Exeter, Exeter, EX4 4QF, UK
[d] School of Engineering, University of Manchester, Manchester, M13 9PL, UK

ARTICLE INFO

Keywords:
Marine launch and recovery (L&R)
Sliding mode observer
Tube-based model predictive control (TMPC)
Collision avoidance

ABSTRACT

This paper investigates a non-causal control scheme for the Marine Launch and Recovery (L&R) systems involving a mothership and a small rigid-hulled inflatable boat (RHIB). The controller is considered non-causal as it requires predicted future wave information for decision-making. The main challenges are: 1) the system is underactuated with the tension force in the connecting cable as the only control input; 2) both mothership and RHIB are subject to uncertain wave-induced disturbances that pose challenges to collision avoidance; 3) the overall system exhibits nonlinear dynamics with coupling between the cable dynamics and the swing dynamics. Traditional Tube-based Model Predictive Control (MPC) addresses these challenges but leads to overly conservative control actions. In this paper, a Sliding Mode Observer (SMO) based MPC is proposed to reduce the conservatism, leading to reduced steady-state errors. Furthermore, the online computational load for the proposed scheme is similar to the traditional MPC, as the SMO is computationally cheap. Numerical simulations have been conducted to verify the effectiveness of the proposed scheme.

1. Introduction

Marine Launch and Recovery (L&R) systems have been extensively studied in the literature for the L&R of Unmanned Aerial Vehicles (UAV) and Unmanned Surface Vehicles (USV) (Nie et al., 2021; Zhang et al., 2020a; Chu et al., 2021), and autonomous or remotely-operated submarines from a mothership (Szczotka, 2022; Tran et al., 2023; Ross et al., 2022; Chen et al., 2020). Typically, manual L&R of marine vessels from a mothership involves a crane connected to a small boat via a cable. During recovery, a trained operator assesses sea state conditions and initiates the hoisting procedure based on their judgment of operational safety. While lifting the boat, the operator monitors the vessel motion to avoid collision with the mothership. The main challenge of this operation is the high-risk that arises because of the environmental conditions such as sea waves, wind, currents. When the small boat is attached to the cable but still on the water, rough sea conditions may induce capsizing. Similarly, significant cable oscillations during hoisting can cause the small boat to collide with the mothership when the boat is out of water. Therefore, manual L&R operation is typically restricted to calm sea states. Related research in Arctic navigation has shown that external environmental factors, such as sea ice thickness and concentration, significantly influence vessel following behaviour, emphasising the importance of environmental modelling in operational decision making (Shu et al., 2025).

Automating the L&R process requires prediction of future wave forces to evaluate collision and capsizing risks. The wave force acting on the small boat depends on both sea surface elevation and vessel hydrodynamic characteristics. Sea surface elevation can be predicted by the Deterministic Sea Wave Prediction (DSWP) algorithm (Al-Ani et al., 2020).This method utilises wave radar measurements to construct a short-term wave prediction model. To cope with model uncertainty, an Adaptive Sliding Mode Observer has been developed, and has been demonstrated to be more effective than a Kalman Filter (Zhang et al., 2020b, 2021). Alternative short-term forecasting approaches include Autoregressive Methods (Chen et al., 2022), Gaussian Process (Shi et al., 2018), and Neural Networks (Pang et al., 2023). For L&R applications, these methods could be utilised as long as the prediction error is considered. Apart from the L&R problem, machine learning approaches such

* Corresponding author.
E-mail address: Yao.Zhang@ucl.ac.uk (Y. Zhang).

https://doi.org/10.1016/j.oceaneng.2025.122354
Received 18 May 2025; Received in revised form 8 July 2025; Accepted 30 July 2025
Available online 12 August 2025

as graph neural networks have recently been employed to predict causation in maritime accidents, offering data-driven insights into accident investigation (Gan et al., 2025).

A problem similar to the L&R operation is anti-swing control of a crane mounted on the ship. This topic has been extensively studied, with a comprehensive review provided in Cao and Li (2020). The standard approach is to utilise Proportional-Integral-Derivative (PID) control due to the simplicity of the scheme. Recently, an advanced combination of Particle Swarm Optimization-PID control was investigated for very rough sea conditions (Bozkurt and Ertogan, 2023). This approach, simulated based on a payload of 5 tons, achieved a swing reduction of 60 %. This enhances safety compared to the scenario where control is disabled. Another widely adopted approach is Sliding Mode Control (SMC) because it has the capability of coping with uncertainties in the system (Qian et al., 2024; Zanjani and Mobayen, 2022). A recent scheme proposes an adaptive SMC scheme with an improved reaching law for a multi-cable-system in Zhao et al. (2024). Compared to a Proportional-Derivative scheme, it offers a 77.5 % improvement in error control for a 10-ton payload.

In this article, the focus is on autonomous L&R of a rescue vessel, specifically a small rigid-hulled inflatable boat (RHIB) to a mothership. To achieve safe and reliable operation, the control system must satisfy several key requirements.First, the cable swing angles must remain small throughout the operation to avoid collision. Second, the control strategy must respect actuation limits, particularly the limitation of the cable tension. Third, the angular velocities must be constrained in the case of human occupation of the RHIB. Finally, the cable length must reduced in such a way that its final velocity is zero. Because in practice, L&R is mostly operated manually, there is limited literature describing the dynamics and control of the process. Zhang et al. (2022) modelled the problem as a 2D underactuated system under Sliding Mode Control (SMC). Their method relies on wave prediction to evaluate the feasibility of the operation. The simulation results show the capability of the controller to shorten the cable while achieving zero terminal velocity. An integral SMC scheme is developed in Rout et al. (2024), and it demonstrates robust success in the presence of rough sea states. To handle constraints and disturbances explicitly, a tube-based Model Predictive Control (TMPC) scheme is applied to a 2D model with consideration of the ship motion response in Zhang et al. (2023b). Although TMPC is robust to disturbances, the conventional TMPC suffers steady-states error in the presence of persistent disturbances. To address this, Zhang et al. (2023a) introduced a Sliding Mode Observer (SMO) to estimate disturbances and compensate for them within the robust MPC framework. In addition, the computational time of the combined TMPC-SMO scheme remains similar, as SMO is computationally cheap. Therefore, this paper will adopt this combined method to enable fully autonomous L&R.

Similar to the previous study (Zhang et al., 2023b, 2022), the control scheme proposed in this work is non-causal. This means that it requires future wave prediction which in turn predicts the motion of the mothership as well as the wave forces acting on the system. This future information was incorporated in the controller for feasibility checks.

While both SMO and TMPC are mature techniques, their systematic combination remains novel. This is because combining a causal method like SMO with a non-causal framework like TMPC requires careful handling of their interplay. Specifically, SMO is capable of providing a known, decreasing bound on the estimation error, which is critical for constructing the invariant tube required by TMPC. This non-causal bound from SMO informs TMPC to have less conservative constraint tightening. Therefore, it improves the control performance by reducing steady-state error in regulation tasks.

This is, to the best of the authors' knowledge, the first attempt to adopt the prior published work in Zhang et al. (2023a) in the context of marine related problems. Moreover, this framework is particularly well-suited to the launch and recovery application, where waves are predictable. Since the SMO provides a noncausal bound on the estimation error, wave prediction can be leveraged to further improve the observer's performance, resulting in a less conservative disturbance bound passed to the TMPC.

The contributions described in this paper are as follows:

a) The proposed control algorithm implements a SMO based MPC scheme from Zhang et al. (2023a) on a nonlinear time-varying system.
b) The proposed control scheme enhances the robustness of marine L&R systems against uncertainties and ensures that collision is avoided through state constraints.
c) The implementation of the SMO in marine L&R reduces the bound of the disturbance that the TMPC has to handle, and thus lowers the steady-state error of the target cable length and velocities. This increases the accuracy of the operation.

The remainder of the article is structured as follows. Section 2 introduces the problem formulation for the L&R system. Then, Section 3 describes the formulation of the controller, observer, and their implementation. Section 4 provides simulation results and analysis. Finally, Section 5 concludes the paper.

2. Problem formulation for L&R system

In this section, the dynamics for the marine L&R system is introduced. The dynamics for the 2D L&R system is taken from Zhang et al. (2022). The reference frames for the system are defined in Fig. 1. They are the earth-fixed frame (O_0, x_0, z_0), mothership-fixed frame (O_1, x_1, z_1),

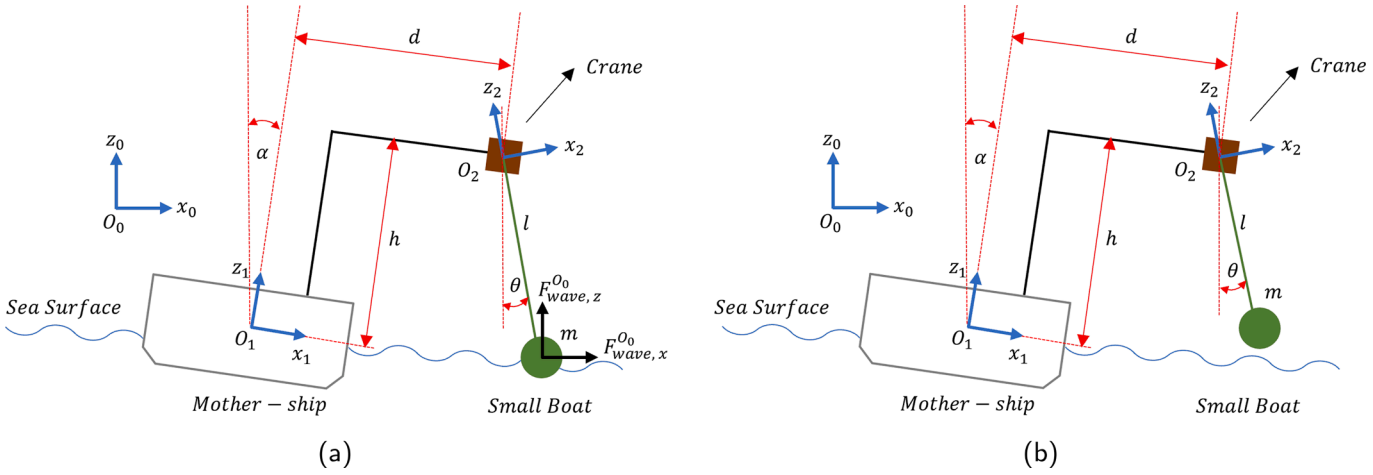

Fig. 1. L&R system diagram. (a) Stage 1 - payload is on the water. (b) Stage 2 - payload is out of the water.

Table 1
Notations.

Notation	Definition
d	Horizontal distance of crane w.r.t O_1
h	Vertical distance of crane w.r.t O_1
m	Mass of the payload
α	Roll angle of the mothership w.r.t O_0
x_m	Horizontal distance of O_1 w.r.t O_0
z_m	Vertical distance of O_1 w.r.t O_0
l	Cable length w.r.t O_0
θ	Swing angle w.r.t O_0
$F_{\text{wave},x}$, $F_{\text{wave},z}$	Horizontal/vertical component of wave forces acting on payload w.r.t O_0
F_T	Cable tension force w.r.t O_0
$\epsilon_\theta, \epsilon_l$	Model uncertainties in the equation of motion w.r.t O_0
g	Gravitational acceleration w.r.t O_0

and payload-fixed frame (O_2, x_2, z_2). There are two stages for the L&R procedure which here are named Stage 1 and Stage 2. The first stage commences when the payload is in the water subject to wave forces. The subsequent stage begins as the payload emerges from the water and it is no longer affected by wave forces. The notations and their corresponding definition are explained in Table 1. The small angle approximation is employed in the dynamic formulation, which remains valid for swing angles within ±10 deg. This assumption is justified, as the system is expected to operate within this range to minimise the risk of collision. Since both stages has similar model form, they can be described as in Eqs. (1)–(5).

$$\ddot{\theta} = -\frac{2\dot{\theta}\dot{l}}{l} - \frac{\theta}{l}g - \frac{1}{l}D_\theta + \epsilon_\theta \tag{1}$$

$$\ddot{l} = -\frac{F_T}{m} + g + \dot{\theta}^2 l + D_l + \epsilon_l \tag{2}$$

where

$$D_\theta = \begin{cases} \theta\bar{\Omega}_z + \bar{\Omega}_x, & \text{if } l \geq l_s \\ \theta\Omega_z + \Omega_x, & \text{if } l < l_s \end{cases} \tag{3}$$

$$D_l = \begin{cases} \bar{\Omega}_z - \theta\bar{\Omega}_x, & \text{if } l \geq l_s \\ \Omega_z - \theta\Omega_x, & \text{if } l < l_s. \end{cases} \tag{4}$$

and

$$\begin{aligned} \bar{\Omega}_x &= \ddot{x}_m + (-\alpha\ddot{\alpha} - \dot{\alpha}^2)d + (\alpha\dot{\alpha}^2 - \ddot{\alpha})h - F_{\text{wave},x}/m \\ \bar{\Omega}_z &= \ddot{z}_m + (-\alpha\dot{\alpha}^2 + \ddot{\alpha})d + (-\alpha\ddot{\alpha} - \dot{\alpha}^2)h - F_{\text{wave},z}/m \\ \Omega_x &= \ddot{x}_m + (-\alpha\ddot{\alpha} - \dot{\alpha}^2)d + (\alpha\dot{\alpha}^2 - \ddot{\alpha})h \\ \Omega_z &= \ddot{z}_m + (-\alpha\dot{\alpha}^2 + \ddot{\alpha})d + (-\alpha\ddot{\alpha} - \dot{\alpha}^2)h. \end{aligned} \tag{5}$$

The symbol l_s in Eqs. (3)–(4) refers to the length at which the payload has been lifted out of the water. In reality, this is a time-varying variable dependent on the wave information (see Remark 1).

Eqs. (1) and (2) can be transformed into a nonlinear control affine state-space model as follows

$$\dot{p} = f(p) + Gu + w \tag{6}$$

where

$$f(p) = \begin{bmatrix} \dot{\theta} \\ \dot{l} \\ -\frac{2\dot{\theta}\dot{l}}{l} - \frac{\theta}{l}g - \frac{1}{l}D_\theta \\ g + \dot{\theta}^2 l + D_l \end{bmatrix}, G = \left[0, 0, 0, -\frac{1}{m}\right]^T, w = \left[0, 0, \epsilon_\theta, \epsilon_l\right]^T \tag{7}$$

In Eq. (6), the states are $p = \left[\theta; l; \dot{\theta}; \dot{l}\right]$ while the control input is u. Both are subject to state constraints, $p \in \mathbb{P}$, and input constraint, $u \in \mathbb{U}$. Similarly, the external disturbance, w, is bounded by the set $\mathbb{W}$. Since the proposed TMPC scheme utilises a discrete system, the state-space model is discretised by the method described in Verschueren et al. (2022).

Remark 1. The variable l_s in Eqs. (3) and (4) represents the cable length at which the payload is lifted out of the water surface. This value is influenced by the time-varying wave elevation. During typical launch and recovery operations, such variations in l_s can be reasonably predicted based on the wave prediction methods. Furthermore, the variation in l_s does not compromise the overall stability of the proposed control system

3. Tube-based model predictive control for launch and recovery system based on sliding mode observer

In this section, a sliding mode observer is presented to address uncertainties within the robust TMPC framework. The combination of the TMPC-SMO method and the constraint tightening technique is introduced. Subsequently, the implementation of the proposed algorithm is discussed in detail.

3.1. Sliding mode observer (SMO) formulation

The main idea of using a SMO is to reduce the disturbance that the TMPC has to handle. This is achieved by compensating the controller with the estimated matched disturbance ($\hat{w}_{ma}$). A SMO was selected to create $\hat{w}_{ma}$ since it has fast convergence and it can provide non-causal information to the MPC. In this subsection, the derivation of $\hat{w}_{ma}$ follows the same approach as in Zhang et al. (2023a). Firstly, the sliding variable s is defined as

$$s = p - \lambda \tag{8}$$

where $\lambda(0)$ is selected to make $s(0) = 0$ and the variable λ is defined as

$$\dot{\lambda} = f(p) + Gu - v(s) \tag{9}$$

with $v(s)$ as the injection signal depending on s. Based on (6), (8), and (9), it follows

$$\dot{s} = \dot{p} - \dot{\lambda} = w + v(s) \tag{10}$$

The ith component of $v(s)$ is chosen as

$$\begin{cases} v_i(s) = -\gamma \operatorname{sign}\left(s_i\right)\left|s_i\right|^{\frac{1}{2}} + \lambda_{0i} \\ \dot{\lambda}_{0i} = -\beta \operatorname{sign}\left(s_i\right) \end{cases} \tag{11}$$

where $\dot{\lambda}_{0i}(0) = 0$, and $\gamma > 0$ and $\beta > 0$ are constant gain parameters. If a new vector $\tilde{\lambda}_0 = \lambda_0 + w$ is defined, then combined with (10), the ith component of $\dot{s}$ can be written in the following super-twisting structure.

$$\begin{cases} \dot{s}_i = \tilde{\lambda}_{0i} - \gamma \operatorname{sign}\left(s_i\right)\left|s_i\right|^{\frac{1}{2}} \\ \dot{\tilde{\lambda}}_{0i} = \dot{w}_i - \beta \operatorname{sign}\left(s_i\right) \end{cases} \tag{12}$$

Moreover, choosing the estimated disturbance as $\hat{w} = -\lambda_0$ yields $\tilde{\lambda}_0 = w - \hat{w}$. Therefore, $\tilde{\lambda}_0$ becomes the estimation error of the disturbance and it is bounded and converges to zero in finite time according to Zhang et al. (2023a). In the case of the L&R system described in (6), $\hat{w}_{ma} = \hat{w}_4 = \hat{\epsilon}_l$. This implies the fourth component of the estimated disturbance, $\hat{w}$.

3.2. Tube-based MPC based on SMO

The purpose of robust TMPC is to constrain the trajectory of the uncertain system inside a tube centered around the nominal trajectory without disturbances. In the controller, the assumption is that full-state measurement is available. To formulate the controller, a nominal L&R model is defined based on (6) without the external disturbance (w): specifically

$$\dot{\bar{p}} = f(\bar{p}) + G\bar{u} \tag{13}$$

where $\bar{p}$ and $\bar{u}$ are the nominal states and nominal control input respectively. The objective of the nominal MPC is to minimise the nominal cost function ($\bar{J}$) described as

$$\bar{J} = \min_{\bar{u}} \sum_{k=1}^{N-1} (\bar{p}(k) - p_r(k))^T Q(\bar{p}(k) - p_r(k)) + \bar{u}^T(k) r \bar{u}(k) \tag{14}$$

where Q and r are the weighting matrices of the states and control input. Moreover, Eq. (14) is subject to the model in (13), and

$$\bar{p} \in \bar{\mathbb{P}} \subset \mathbb{P},\ \bar{u} \in \bar{\mathbb{U}} \subset \mathbb{U},\ p_r \in \mathbb{P}_r, \bar{\mathbb{P}} = \mu_1(k)\ \mathbb{P},\ \bar{\mathbb{U}} = \mu_2(k)\ \mathbb{U}_{mpc} \tag{15}$$

where N is the prediction horizon length, both $\bar{p}$ and $\bar{u}$ are constrained by the tightened set $\bar{\mathbb{P}}$ and $\bar{\mathbb{U}}$, and the reference trajectory (p_r) is also bounded by the set $\mathbb{P}_r$. The scalars, $\mu_1(k)$ and $\mu_2(k)$, are positive time-varying parameters that tighten the constraint set $\mathbb{P}$ and $\mathbb{U}_{mpc}$. This is to ensure the constraint satisfaction of the uncertain system over the bounded disturbance sequence Mayne et al. (2011). In addition, the constraint set $\mathbb{U}_{mpc}$ is a tightened constraint set from the original constraint $\mathbb{U}$ based on the compensation from the SMO.

$$\mathbb{U}_{mpc} := \left\{u_{mpc} \in R^{n_u} : |u_{mpc}| \leq u_{max} - m\hat{w}_{ma,max}\right\} \tag{16}$$

where n_u is the dimension of the control input, $u_{\max}$ is the maximum value of the original bound for the control input and $w_{ma,\max}$ is the maximum value of the matched disturbance. Unlike in the typical nonlinear TMPC, the nominal constraint set is time-varying as the SMO indirectly provides information about the size of the set. This reduces the conservatism of the solution while ensuring constraint satisfaction. The procedure to calculate the tightening parameters is discussed in Remark 2. The solution of the optimisation problem in (14) is a sequence of nominal control inputs calculated at timestep k, $\bar{\mathbf{u}} = [\bar{u}(k), \bar{u}(k+1), \ldots, \bar{u}(k+N-1)]^T$. The applied control input at timestep k to the nominal system is $\bar{u}^* = \bar{u}(k)$, and it results in the nominal states $\bar{p}^* = \bar{p}(k)$. Then, $\bar{\mathbf{u}}$ is recalculated for the next timestep.

To enhance the robustness of the uncertain system against disturbances, an ancillary controller is implemented. The ancillary controller maintains the trajectories of the uncertain system revolving around the nominal system bounded by a tube. It is achieved by introducing a cost function as follows

$$\begin{aligned} J = \min_{u_{mpc}} & \sum_{k=1}^{N-1} (p(k) - \bar{p}^*(k))^T Q (p(k) - \bar{p}^*(k)) \\ & + (u_{mpc}(k) - \bar{u}^*(k))^T r (u_{mpc}(k) - \bar{u}^*(k)) \end{aligned} \tag{17}$$

The minimization in (17) is also subject to

$$p \in \mathbb{P},\ u_{mpc} \in \mathbb{U}_{mpc} \tag{18}$$

and the dynamical system in (6) without the external disturbances. In the ancillary controller calculation, the disturbance (w) is omitted from the uncertain system (6) and the deviation of the uncertain trajectory is stabilised by the resultant controller. Similar to the nominal controller, the solution of the optimisation problem in (17) is a sequence of robust control inputs calculated at timestep k, $\mathbf{u_{mpc}} = \left[u_{mpc}(k), u_{mpc}(k+1), \ldots, u_{mpc}(k+N-1)\right]^T$ and the resulting control input at timestep k is $u^*_{mpc} = u_{mpc}(k)$.

Remark 2. In the nonlinear TMPC problem, the constraint set ($\bar{\mathbb{P}}, \bar{\mathbb{U}}$) is tightened by a constant scalar parameter found by utilising Monte Carlo simulation Mayne et al. (2011). However, in the current TMPC-SMO problem, the tightened constraint set is time-varying as a result of the control input compensation from the SMO. Therefore, a modified strategy to find the time-varying parameter is introduced as follows

1. Before the tightened set is calculated, the time-varying parameters are held constant, $\mu_1 = \mu_2 = 1$.
2. Monte Carlo simulation is employed for the closed-loop system with the compensation from the SMO for various disturbance sequences. The maximum resultant spread of trajectories ($2d_{p,k}$ and $2d_{u,k}$) is calculated for each state and control input.
3. For time step k, the constraints for each nominal state and control input is tightened by $d_{p,k}$ and $d_{u,k}$ respectively.
4. Set the current timestep to k+1, Steps a) to c) are then repeated until the timestep reaches the end of simulation horizon (N_s).

Remark 3. As explained in Remark 2, the tightening parameters (μ_1 and μ_2) are computed offline using Monte Carlo simulations, as described in Mayne et al. (2011). While adaptive or generalised tightening methods are possible, they typically rely on strong assumptions or bounds. Moreover, the Launch and Recovery system considered in this study operates within a relatively narrow region. Introducing additional assumptions or bounds can lead to unnecessary conservatism and potentially degrade the optimality of the control performance. The Monte Carlo-based approach offers a practical alternative, since they do not require additional assumptions or bound. Moreover, the computational burden is manageable offline with standard computer.

Remark 4. The stability and feasibility of the TMPC scheme can be imposed by adding a terminal cost and constraint with the standard proof for nonlinear TMPC from Mayne et al. (2011)

The tuning parameters of the nonlinear TMPC are as follows Mayne et al. (2011): 1) the weighting gains, Q and r, these gains could be tuned separately for the nominal and robust MPC to give a better performance in attenuating the disturbances; 2) The prediction horizon step (N), could be reduced in the ancillary controller for faster computational time but the prediction horizon time should not be altered; 3) The prediction horizon time could be tuned but the duration generally depends on the timescale of the particular system dynamics and disturbances.

3.3. Implementation

The implementation of the TMPC-SMO in the L&R operation is described in Algorithm 1 and Fig. 2. To combine the TMPC and the SMO, the resulting compensated control input (u) applied to the system takes the form

$$u = u_{mpc} + m\hat{w}_{ma} \tag{19}$$

Algorithm 1 TMPC based SMO for marine L&R control.

1: **Initialisation:** model parameters, initial states (p_0), TMPC weight parameters (Q, r), constraints set ($\mathbb{P}, \mathbb{U}$), constraints tightening parameters (μ_1, μ_2), SMO parameters (γ, β).
2: **Wave Prediction:** reset the current time to be zero, predict the sea wave and mothership response to give ($\bar{\Omega}_x, \bar{\Omega}_z, \Omega_x, \Omega_z$).
3: **for** i **from** 0 **to** simulation horizon (N_s), **do**
4: **Nominal control:** compute the nominal state $\bar{p}$ and control input $\bar{u}$ over $\left[t_i, t_i + N_s T_s\right]$.
5: **SMO:** for given p and u, use the observer to find $\hat{w}_{ma}$
6: **TMPC-SMO:** using Monte Carlo simulations, compute the actual system states p and control input u_{mpc} that will be compensated by the observer so that $u = u_{mpc} + m\hat{w}_{ma}$ over $\left[t_i, t_i + N_s T_s\right]$.
7: **Constraint tightening parameters update:** at each time step (t_i), calculate the maximum resultant spread of the trajectories and update the $\mu_1(i), \mu_2(i)$
8: **end for**
9: **Constraint set update:** update the nominal constraint set to be $\bar{\mathbb{P}} = \mu_1(i)\ \mathbb{P}, \bar{\mathbb{U}} = \mu_2(i)\ \mathbb{U}_{mpc}$
10: **Nominal control with tightened constraint:** run the nominal control with constraint set $\bar{\mathbb{P}}, \bar{\mathbb{U}}$, and check if the MPC is feasible.
11: **if** Nominal control with tightened constraint is feasible, **then**
12: **Robust TMPC-SMO:** check the feasibility of the scheme via simulation over all the uncertain disturbances sequence
13: **else** repeat step 2 when 0.5 s has passed
14: **end if**
15: **Real-time implementation:** using step 10 as the reference trajectory, compute the MPC control input u, the observed disturbance $\hat{w}_{ma}$ online, and transmits the compensated control input to the L&R System

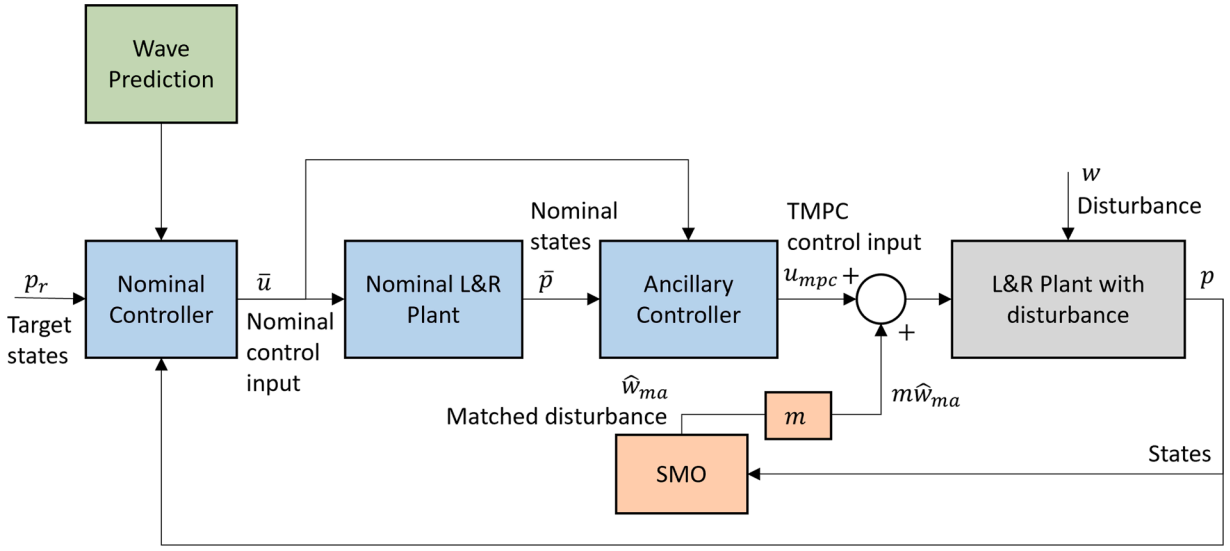

Fig. 2. TMPC-SMO control scheme for real-time L&R system.

Table 2
Simulation parameters.

Parameter	Notation	Value
Mass of the payload	m	1040 kg
TMPC sampling time	$T_{s,mpc}$	0.1 s
Prediction horizon	N	20 steps
Simulation horizon	N_{sim}	50 steps
weighting matrix of states	Q	diag(0, 2000, 0.5, 1500)
weighting matrix of input	r	3×10^{-5}
SMO sampling time	$T_{s,smo}$	0.0001 s
SMO parameter	γ, β	1,1

This compensation reduces the bound of disturbance that the TMPC has to handle. As it decreases, the resulting steady-state error reduces. In addition, a feasibility check is proposed to verify the feasibility of MPC. If it is not feasible, for instance, due to harsh wave conditions, the controller will wait for 0.5 s before checking the feasibility again.

4. Numerical results and discussion

In this section, the results of the simulation for the proposed control scheme are presented. The simulation framework is first introduced, followed by a performance evaluation of the SMO. The analysis is divided into two parts. In Part 1, the performance of the proposed TMPC-SMO scheme is compared against the TMPC. Relevant performance metrics are defined, and the TMPC-SMO is further assessed under varying levels of mothership motion prediction error to evaluate its robustness. In Part 2, a Monte Carlo simulation is conducted across different initial conditions to examine the robustness of the control scheme.

The simulation was excecuted in Matlab with an Intel i7-7500U CPU. For the MPC optimisation calculations, acados was utilised (Verschueren et al., 2022) which offers high-performance fast optimization that can be directly implemented for embedded applications. The nonlinear optimal control problem from MPC is discretised using the multiple shooting approach as it has good convergence. Then, for fast real-time application, the problem is converted to a Sequential Quadratic Problem (SQP). To implement this, a QP sub-problem is defined and solved efficiently by a high-performance interior-point method (HPIPM) solver from Frison and Diehl (2020).

Table 2 shows the parameters that are utilised in the simulation. The gains for the SMO (γ, β) are designed such that $s_i = \dot{s}_i = 0$ in Eq. (12) in finite time (Nagesh and Edwards, 2014). While increasing these gains accelerates the convergence of the prediction error, it may also amplify chattering. Therefore, a trade-off exists, and the tuning is performed to achieve a balance between convergence speed and chattering. Based on the simulation horizon and sampling time, the total time of the simulation is 5s. This is chosen because a larger time window in real-time L&R may cause the system to encounter a larger wave train which will affect the feasibility of the controller. Although this could be avoided by conducting a feasibility check, in this simulation, it is assumed that the feasibility of the mission has already been checked and the L&R control scheme is ready to be deployed. The gains (Q, r) of the TMPC are designed such that cable length can be decreased to the target in under 5 s. For the gain related to the swing angle and its derivative, it was chosen to be small as the system is underactuated in these states. Here, for convenience, the parameters of the MPC are identical for both nominal and ancillary controller.

For safe L&R operation, the constraint for the states and control input of the TMPC scheme are given in (20). This is based on the literature in Zhang et al. (2022) and they are defined to avoid collision with mothership. The initial conditions of the states are $p_0 = [4 \text{ deg}; 6 \text{ m}; 0 \text{ deg/s}; 0 \text{ m/s}]$, and the target states are $p_r = [0 \text{ deg}; 4 \text{ m}; 0 \text{ deg/s}; 0 \text{ m/s}]$.

$$\begin{bmatrix} -10 \text{ deg} \\ 0 \text{ m} \\ -10 \text{ deg/s} \\ -1.6 \text{ m/s} \end{bmatrix} \leq p \leq \begin{bmatrix} 10 \text{ deg} \\ 10 \text{ m} \\ 10 \text{ deg/s} \\ 1.6 \text{ m/s} \end{bmatrix} \tag{20}$$
$$|u| \leq 15,000 \text{ N}$$

The external disturbances (w) due to modelling, wave prediction errors, wind, and current disturbances are assumed to be sinusoidal functions as described below

$$\begin{aligned} w_3 &= \epsilon_\theta = A_{\epsilon_\theta} \sin at \\ w_4 &= \epsilon_l = A_{\epsilon_l} \sin at. \end{aligned} \tag{21}$$

where, for each Monte Carlo iteration, the amplitude of the disturbance is a randomly selected constant $A_{\epsilon_\theta} \sim \mathcal{N}(0, 0.5)$, $A_{\epsilon_l} \sim \mathcal{N}(0, 0.5)$ and the frequency of the sinusoidal function is $a = 1$.

The result of the SMO on one of the Monte Carlo simulation is shown in Fig. 3(a). It can be observed that the estimated disturbance is in good agreement with the actual disturbance. The estimation error also converges to almost zero in under one second. As the L&R operation is under 5 s, fast convergence of the estimation error is highly beneficial. Additional simulations of the SMO with an initial prediction error of 0.2 are presented in Fig. 3(b). The observer converges in less than 0.1,s,

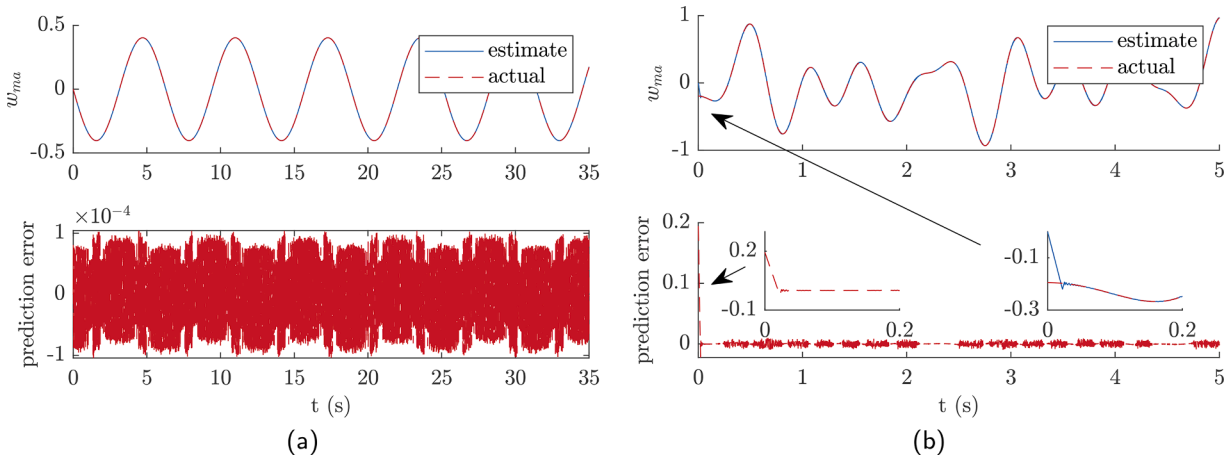

Fig. 3. Sliding mode observer performance to estimate matched disturbance. (a) $\hat{w}_{ma} = w_4$ and the estimation error ($w_{ma} - \hat{w}_{ma}$) with $A_{\epsilon_i} = -0.403$ for one of the Monte Carlo simulation. (b) initial estimation is different from the actual matched disturbance.

indicating that initial estimation errors have minimal impact on its performance.

The complete simulation of the proposed scheme is divided into two parts:

1. *Part 1*: Comparison of the proposed TMPC-SMO scheme with a traditional nonlinear TMPC without the observer.
2. *Part 2*: Monte Carlo simulation of the proposed TMPC-SMO scheme with various initial states to demonstrate the robustness of the scheme.

In Part 1 of the simulation, TMPC-SMO scheme is compared with traditional nonlinear TMPC without an observer. It is important to clarify that this paper does not aim to benchmark the SMO against other observer designs. Rather, the focus is on demonstrating that only the SMO makes the proposed integration with Tube-based MPC (TMPC) feasible in the current formulation. This is because the SMO can be designed to provide a known and decreasing bound on the estimation error that can construct an invariant tube for TMPC. This approach follows the same rationale outlined in previous work published in Zhang et al. (2023a). Therefore, comparisons with other observer methods are not included, as they fall outside the scope of this specific contribution.

Figs. 4–7 show the comparison of the TMPC-SMO and TMPC schemes with 40 Monte Carlo simulations. The blue vertical line separates the two stages i.e. when the small boat is on or out of water, while the green dotted line represents the constraints. Since the system is underactuated, it is not possible to bring the angle to the target angle. Therefore, both the swing angle and the angular velocities are oscillatory. Nevertheless, the constraints are respected by the states and this shows the advantage of utilising the proposed control scheme to avoid a small boat collision with the mothership (even if the system is underactuated). For both length and velocity, the TMPC-SMO scheme shows minimal deviation from the nominal control trajectory compared to the TMPC scheme. This demonstrates its ability to eliminate matched disturbances and it reduces the steady-state error of the system. All the schemes also complete the operation in under 5s which is acceptable for a L&R mission.

The control input for the simulation is shown in Fig. 8. Similar to the states, the input is within the constraint of 15000 N which is acceptable. However, the constraint in the TMPC-SMO is not active as a result of multiple constraint tightening through the Monte Carlo method and the compensation provided by the SMO.

The numerical performance of the controller can be quantified using a RMSE method as follows

$$\text{RMSE} = \sqrt{\frac{\sum_{i=k}^{N_{sim}} \left(n_i - n_r\right)^2}{N_{sim} - k + 1}} \tag{22}$$

Table 3
RMSE and maximum steady state error from the simulation.

States	RMSE ($k = 45$)		Maximum value	
	TMPC-SMO	TMPC	TMPC-SMO	TMPC
θ	3.66 deg	3.63 deg	5.58 deg	5.56 deg
l	0.0065 m	0.025 m	0.01 m	0.06 m
$\dot{\theta}$	6.81 deg/s	6.68 deg/s	8.68 deg/s	8.56 deg/s
$\dot{l}$	0.016 m/s	0.025 m/s	0.03 m/s	0.066 m/s

where k is the starting timestep for the performance calculation, n_i denotes the i-th value of the variable and n_r is the target variable. The RMSE for each state are presented in Table 3 where the RMSE is calculated for the last half-second of the simulation ($k = 45$). The results suggest that the RMSE of the cable length for the TMPC-SMO is 0.0065 m while the TMPC only achieves 0.025 m. This could be considered as the steady-state error and it demonstrates that the TMPC-SMO scheme manages to improve the tracking performance and reduce the error for the states that have matched disturbances. Moreover, the RMSE of the swing angle and angular velocity remains within the constraints, ensuring the safety of the proposed control scheme. In addition to the RMSE calculations, the maximum value of the last half-second of the simulation is also investigated in Table 3. It shows that the TMPC-SMO is effective in reducing the maximum steady state error of the cable length compared to TMPC.

Apart from the RMSE analysis, three additional performance metrics used are the Control Effort (CE), computation time, and the Integral of Time-weighted Absolute Error (ITAE). The Control Effort quantifies the total energy of control actions applied over the simulation, computed as the sum or integral of squared control inputs, which is defined as follows

$$\text{CE} = \sum_{k=1}^{N_{sim}} |u(k)|^2 \Delta t \tag{23}$$

where Δt is the sampling time. On the other hand, ITAE is calculated with respect to the nominal trajectory to highlight the tracking performance of the scheme. This metric penalises errors that persist over time and is defined as:

$$\text{ITAE} = \sum_{k=1}^{N_{sim}} t(k)|e(k)|\Delta t \tag{24}$$

where $e(k)$ is the error between the nominal trajectory and the robust control trajectory. Table 4 presents a quantitative comparison between the TMPC and the proposed TMPC-SMO controller in multiple performance metrics. In terms of tracking accuracy, the ITAE values for l and

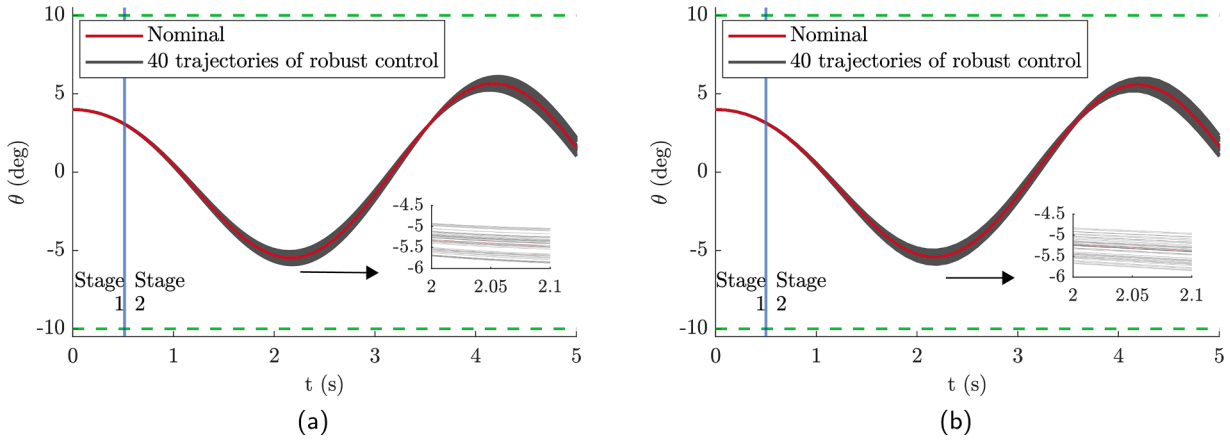

Fig. 4. Nominal control and 40 Monte Carlo robust control trajectories of the swing angle, $|\theta| \leq 10$ deg. (a) TMPC-SMO. (b) TMPC.

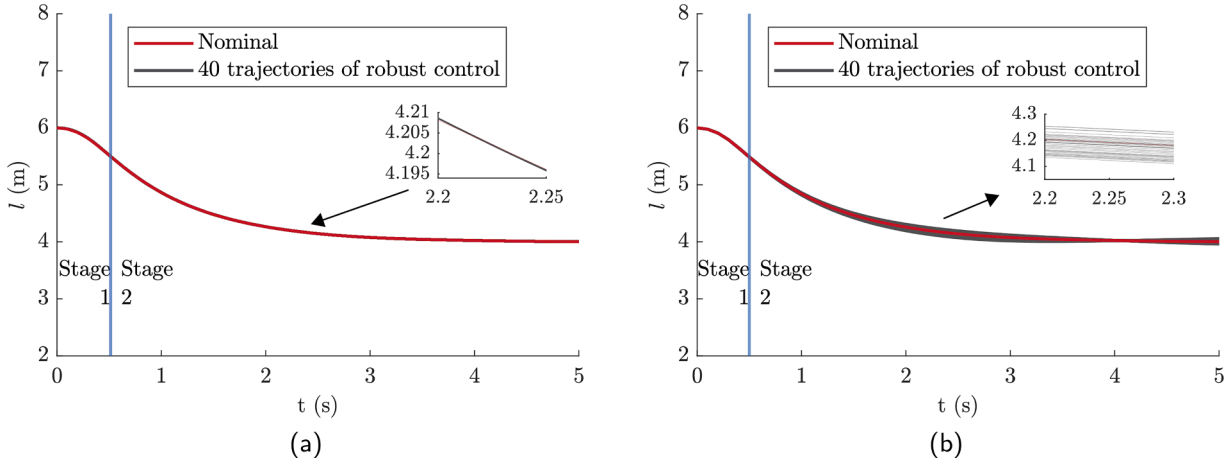

Fig. 5. Nominal control and 40 Monte Carlo robust control trajectories of the cable length, $0\text{m} \leq l \leq 10$ m. (a) TMPC-SMO. (b) TMPC.

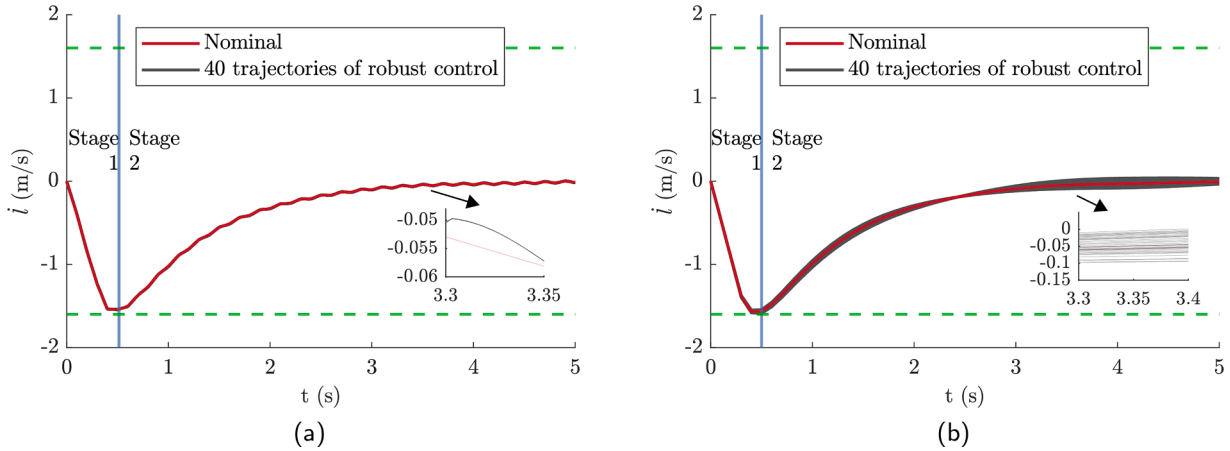

Fig. 6. Nominal control and 40 Monte Carlo robust control trajectories of the cable velocity, $|\dot{l}| \leq 1.6$ m/s. (a) TMPC-SMO. (b) TMPC.

$\dot{l}$ are significantly lower in TMPC-SMO compared to TMPC, indicating improved disturbance attenuation and better trajectory tracking of the nominal path. Meanwhile, the ITAE values for θ and $\dot{\theta}$ remain similar between both approaches. This suggests that the proposed scheme does not adversely affect the angular dynamics.

Regarding the control effort, TMPC-SMO increases the cost to approximately 0.1 % relative to TMPC. This slight increase can be justified by the added compensation term, which increases the actuation commands. However, the difference is negligible and remains within actuator limits. Furthermore, the average computation time required to solve the optimisation problem in (17) and (18) is also included in the table and is presented as a boxplot in Fig. 9. Although TMPC-SMO shows slightly longer mean computation time, both methods achieve solution times well below the MPC sampling interval of 0.1 s. This demonstrates the feasibility of deploying the controller in a real-time setting.

Additional simulations are conducted to evaluate the performance of the proposed TMPC-SMO scheme under varying wave prediction errors. The prediction error is introduced as an error to the predicted

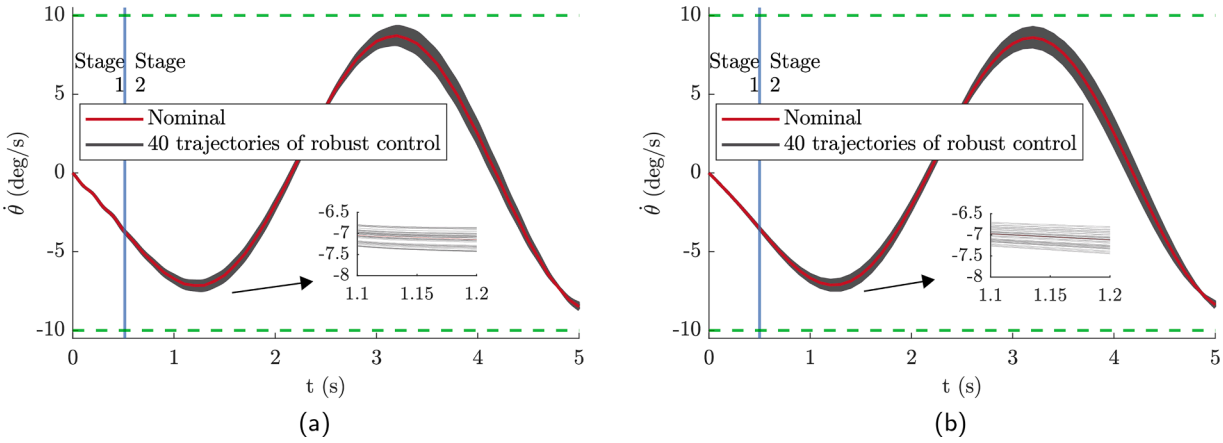

Fig. 7. Nominal control and 40 Monte Carlo robust control trajectories of the swing angular velocity, $|\dot{\theta}| \leq 10$ deg/s. (a) TMPC-SMO. (b) TMPC.

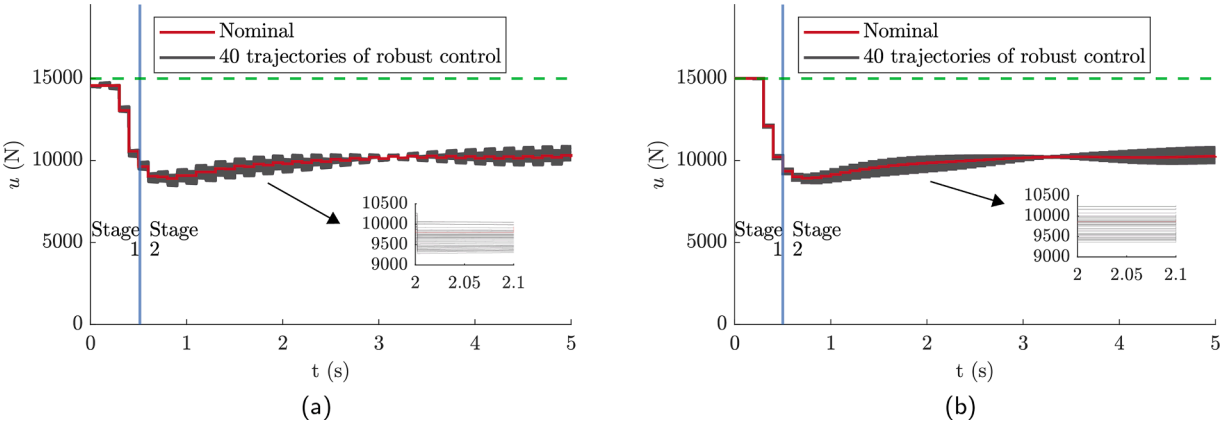

Fig. 8. Nominal control and 40 Monte Carlo robust control trajectories of the control input, $|u| \leq 15,000$ N. (a) TMPC-SMO. (b) TMPC.

Table 4
Comparison of TMPC and TMPC-SMO performance based on ITAE, mean computation time, and CE.

Metric	TMPC	TMPC-SMO
ITAE θ	2.2406	2.2656
ITAE l	**0.2073**	**0.0032**
ITAE $\dot{\theta}$	2.5047	2.3998
ITAE $\dot{l}$	0.2417	0.0351
Control Effort (CE)	5.319×10^8	5.324×10^8
Mean Computation Time (ms)	0.821	1.243

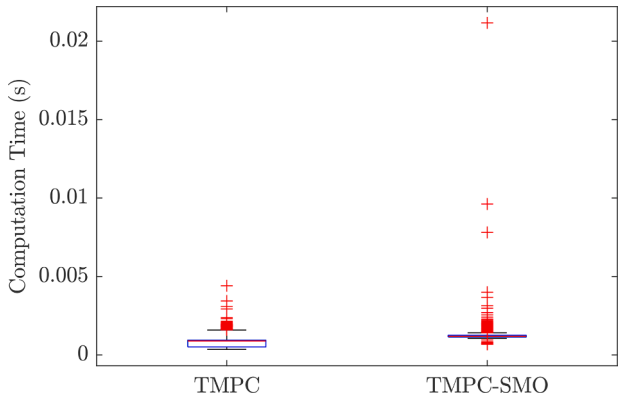

Fig. 9. Boxplot of the online computation time for TMPC-SMO and TMPC. Red line is the median.

mothership motion terms ($\bar{\Omega}_x$, $\bar{\Omega}_z$, Ω_x, Ω_z), defined as $\Omega = \Omega\big(1 + \mathcal{N}(0, \sigma)\big)$, where $\mathcal{N}(0, \sigma)$ is a Gaussian distribution with zero mean and standard deviation σ. In addition, Gaussian noise is injected into the signal with three different signal-to-noise ratios, SNR, (0 dB, 10 dB, 20 dB). These levels were chosen because they sufficiently capture the typical range of noise magnitudes encountered in short-term wave prediction (a few seconds of prediction horizon). Moreover, three prediction standard deviations were tested with $\sigma = 0.05, 0.1, 0.2$.

The resulting ITAE values are shown in Fig. 10 as a boxplot. The results show that the ITAE for θ and $\dot{\theta}$ remains relatively similar to changes in SNR and prediction error. In contrast, the ITAE for l and $\dot{l}$ increases with larger prediction errors and lower SNRs, as expected due to more erroneous predicted motion. Nevertheless, the maximum ITAE values for l and $\dot{l}$ remain around 0.63 and 0.71, respectively, which are within acceptable values. Performance only degrades slightly due to the strong robustness of the TMPC. By incorporating SMO, robustness against wave prediction error is fully considered.

In Part 2, Monte Carlo simulations with different initial conditions for cable length and swing angle are investigated. The variations are ±10 % for the swing angle and ±4 % for the cable length. Combinations of four initial swing angles and four initial cable lengths are investigated with 16 various disturbance sequences. The number of disturbance sequences is less than previously to save computational time. In total, there are $4 \times 4 \times 16 = 256$ trajectories to validate the robustness of the TMPC-SMO scheme. All the controller and observer parameters are the same as previously except for the constraint of cable length velocities. This constraint was relaxed to ±3 m/s but it remains within a reasonable range for L&R. The simulation results are presented in Figs. 11 and 12. The separation line between Stage 1 and Stage 2 is not included, as

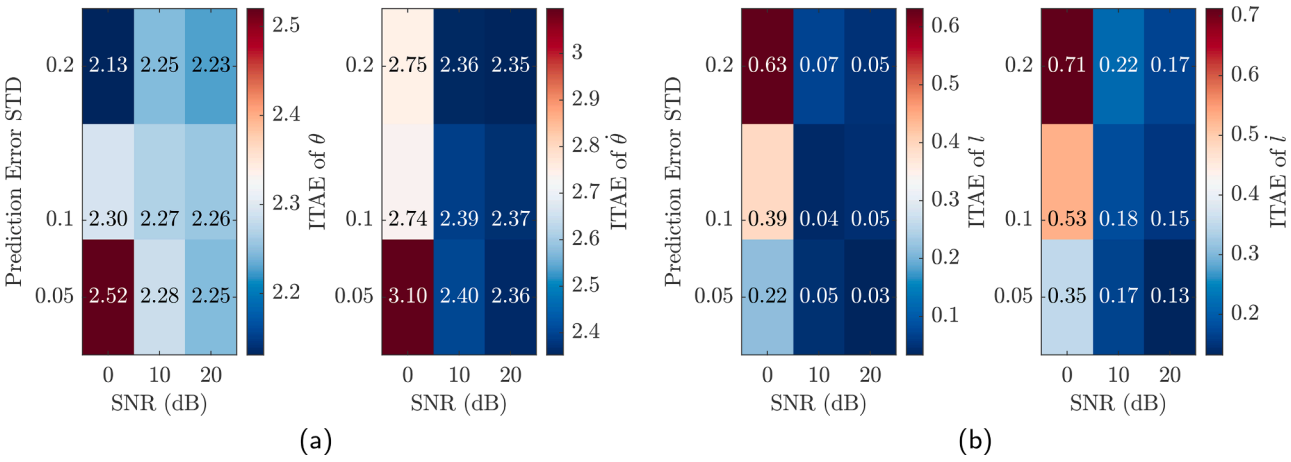

Fig. 10. Boxplot of ITAE for TMPC-SMO with different SNR and prediction std. (a) θ and $\dot{\theta}$. (b) l and $\dot{l}$.

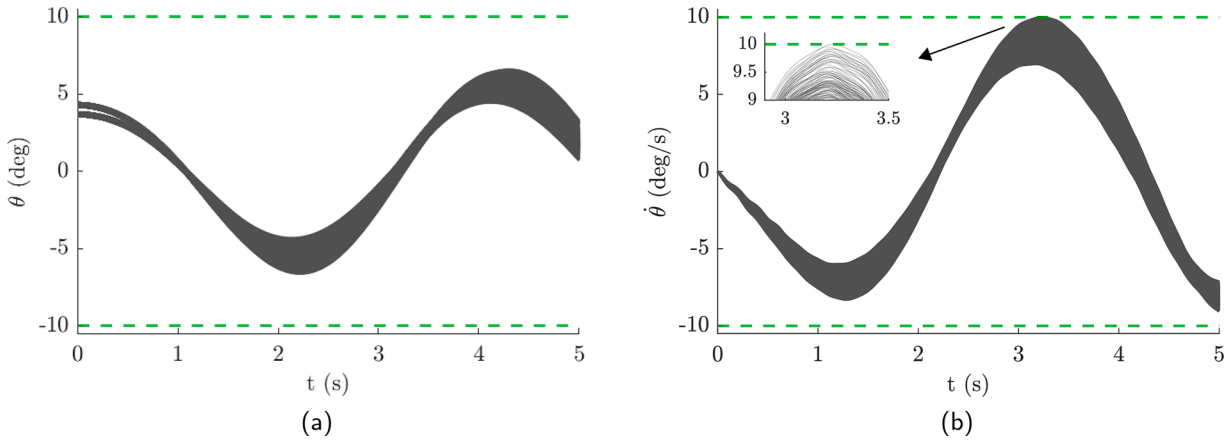

Fig. 11. 256 Monte Carlo robust control trajectories with different initial conditions and disturbance sequences. (a) swing angle, θ. (b) swing angle velocity, $\dot{\theta}$.

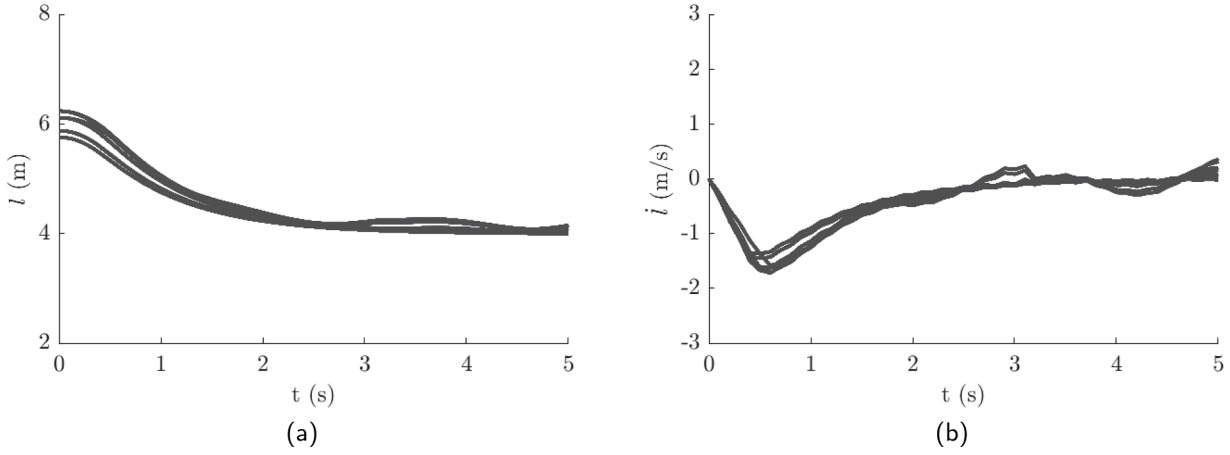

Fig. 12. 256 Monte Carlo robust control trajectories with different initial conditions and disturbance sequences. (a) cable length, l. (b) cable length velocity, $\dot{l}$.

variations in initial conditions result in small differences in the time required to extract the RHIB from the water. It can be observed that the cable length successfully achieves the target in all trajectories. Additionally, all state constraints were respected, indicating that no collision occurs. In particular, the swing angle velocity constraint is active in Fig. 11(b). The results in Table 5 indicate that the mean values of θ and $\dot{\theta}$ remain within the specified constraints at the final simulation step. Meanwhile, the mean values of l and $\dot{l}$ are close to their respective targets of 4 m and 0 m/s. Despite varying initial conditions, the standard deviations remain small across all states, indicating that the controller has limited sensitivity to initial states variation.

It is important to note that the proposed approach relied on a 2D model. The use of a 2D model in the xz-plane with roll dynamics was justified by typical launch and recovery conditions, where the ship is oriented bow- or stern-on to the waves to reduce motion and prevent sea sickness. In this orientation, most excitation occurs in the pitch

Table 5
Mean and standard deviation of the Monte Carlo simulation with different initial conditions. The values are computed at the final step of the simulation.

States	mean	std
θ (deg)	1.7411	0.5102
$\dot{\theta}$ (deg/s)	-8.2140	0.5043
l (m)	4.0352	0.0526
$\dot{l}$ (m/s)	0.0629	0.1270

direction, where oscillations are minimal due to the ship's large moment of inertia. As the crane is mounted on the side, roll becomes the critical angle for collision avoidance. Therefore, selecting the roll angle as the 2D model is justified. Although yaw motion can affect the small boat's orientation, it is generally uncontrollable in single-point recovery unless a mechanical locking mechanism is implemented at the crane tip. Effects outside the 2D plane can be lumped into the disturbance term, ϵ, and compensated through the robust control design. Extending the framework to a full 3D dynamic model, including yaw and lateral forces, remains a relevant direction for future research.

For real-time implementation, several practical considerations must be addressed. The current control design assumes full-state availability. In practical marine environments, not all states are directly measurable, and sensor measurements are subject to noise. To address this, a state observer such as the Extended Kalman Filter (EKF) can be integrated to estimate unmeasured states while accounting for sensor noise and measurement uncertainty. Additionally, the current controller outputs force commands, whereas in actual launch and recovery scenarios, the actuator responsible for generating this force is an electric motor. Most motors, however, are designed to control position or speed rather than force directly. Consequently, an additional transmission system must be modeled and controlled. This includes linking the electric signal through the motor, gearbox, and drum, and ultimately to the pulley cable so that the commanded force can be realised as cable tension force.

5. Conclusions

This paper investigated a robust TMPC-SMO scheme for marine L&R in the presence of external disturbances from wind, current, prediction, and model error. The proposed scheme checks the feasibility of the controller with the future wave prediction before commencing the mission. The proposed disturbance observer converges in finite time with small estimation error. Moreover, the combined controller and observer achieved safe recovery within 5s with a very small cable length error. Future work will focus on refining the model to account for 3D effects (yaw and pitch motion), crane dynamics, and implementation of the controller in a hardware simulator or scaled prototype system.

CRediT authorship contribution statement

Vincentius Versandy Wijaya: Writing – original draft, Visualization, Investigation; **Yao Zhang:** Writing – review & editing, Supervision, Methodology, Conceptualization; **Christopher Edwards:** Writing – review & editing, Methodology, Conceptualization; **Guang Li:** Writing – review & editing, Methodology, Conceptualization; **Michael Belmont:** Writing – review & editing, Methodology, Conceptualization.

Declaration of competing interest

The authors declare that they have no known competing financial interests or personal relationships that could have appeared to influence the work reported in this paper.

Acknowledgement

This work was funded by Wave Energy Scottland Direct Generation Competition and the UK Royal Society IEC-NSFC (223485).

References

Al-Ani, M., Belmont, M., Christmas, J., 2020. Sea trial on deterministic sea waves prediction using wave-profiling radar. Ocean Eng. 207, 107297.
Bozkurt, B., Ertogan, M., 2023. Heave and horizontal displacement and anti-sway control of payload during ship-to-ship load transfer with an offshore crane on very rough sea conditions. Ocean Eng. 267, 113309.
Cao, Y., Li, T., 2020. Review of antiswing control of shipboard cranes. IEEE/CAA J. Autom. Sin. 7 (2), 346–354.
Chen, J., Zhao, W., Milne, I., Draper, S., 2022. Short-term forecasting of surface wave elevation based on an autoregressive model. In: ASME 2022 41st International Conference on Ocean, Offshore and Arctic Engineering. Vol. 5B: *Ocean Engineering of International Conference on Offshore Mechanics and Arctic Engineering*.
Chen, Y., Ma, L., Duan, W., Liu, P., 2020. Experimental study on coupled motions of mother ship launching and recovering of human-occupied vehicle in regular waves. J. Mar. Sci. Appl. 19 (1), 53–63.
Chu, L., Gu, F., Chen, C., Nie, H., Zhang, M., Du, X., He, Y., 2021. Theoretical and experimental study of adaptive control for fixed-wing UAV arrested recovery on the USV. In: 2021 IEEE International Conference on Real-time Computing and Robotics (RCAR), pp. 1329–1334.
Frison, G., Diehl, M., 2020. Hpipm: a high-performance quadratic programming framework for model predictive control. IFAC-PapersOnLine 53 (2), 6563–6569. 21st IFAC World Congress.
Gan, L., Gao, Z., Zhang, X., Xu, Y., Liu, R.W., Xie, C., Shu, Y., 2025. Graph neural networks enabled accident causation prediction for maritime vessel traffic. Reliab. Eng. Syst. Saf. 257, 110804.
Mayne, D.Q., Kerrigan, E.C., van Wyk, E.J., Falugi, P., 2011. Tube-based robust nonlinear model predictive control. Int. J. Robust Nonlinear Control 21 (11), 1341–1353.
Nagesh, I., Edwards, C., 2014. A multivariable super-twisting sliding mode approach. Automatica 50 (3), 984–988.
Nie, H., Zhang, M., Gu, F., Chu, L., Zhang, G., Du, X., He, Y., 2021. Fully automated control system for recovery of fixed-wing UAV. In: 2021 IEEE International Conference on Robotics and Biomimetics (ROBIO), pp. 1642–1649.
Pang, T.Y., Ding, B., Liu, L., Sergiienko, N., 2023. Short-term sea surface elevation prediction using deep learning methods. In: ASME 2023 42nd International Conference on Ocean, Offshore and Arctic Engineering. Vol. 5: *Ocean Engineering of International Conference on Offshore Mechanics and Arctic Engineering*.
Qian, Y., Zhang, H., Hu, D., 2024. Finite-time neural network-based hierarchical sliding mode antiswing control for underactuated dual ship-mounted cranes with unmatched sea wave disturbances suppression. IEEE Trans. Neural Netw. Learn. Syst. 35 (9), 12396–12408.
Ross, J., Sangster, J., Seto, M., 2022. Autonomous recovery of underway AUV on the water surface in heavy seas. In: 2022 IEEE Canadian Conference on Electrical and Computer Engineering (CCECE), pp. 130–135.
Rout, V., Vile, L., Edwards, C., Belmont, M.J., Li, G., Taunton, D., 2024. Control of the launch and recovery of small boats to a mothership in high sea states using sliding mode methods. Control Eng. Pract. 146, 105866.
Shi, S., Patton, R.J., Liu, Y., 2018. Short-term wave forecasting using gaussian process for optimal control of wave energy converters. IFAC-PapersOnLine 51 (29), 44–49. 11th IFAC Conference on Control Applications in Marine Systems, Robotics, and Vehicles CAMS 2018.
Shu, Y., Huang, F., Wu, J., Chen, J., Song, L., Gan, L., Yang, Z., 2025. Research on ship following behavior based on data mining in arctic waters. IEEE Trans. Intell. Transp. Syst. 26 (5), 6778–6788.
Szczotka, M., 2022. Auv launch recovery handling simulation on a rough sea. Ocean Eng. 246, 110509.
Tran, C., Gushkov, I., Nordvik, K., Røang, S.T., Lysthaug, S.B., Ommani, B., Fossen, T.I., Hassani, V., Smines, V., Johansen, T.A., 2023. Operability analysis of control system for ROV launch-and-recovery from autonomous surface vessel. Ocean Eng. 277, 114272.
Verschueren, R., Frison, G., Kouzoupis, D., Frey, J., van Duijkeren, N., Zanelli, A., Novoselnik, B., Albin, T., Quirynen, R., Diehl, M., 2022. acados – a modular open-source framework for fast embedded optimal control. Math. Program. Comput. 14 (1), 147–183.
Zanjani, M.S., Mobayen, S., 2022. Anti-sway control of offshore crane on surface vessel using global sliding mode control. Int. J. Control 95 (8), 2267–2278.
Zhang, H., He, Y., Li, D., Gu, F., Li, Q., Zhang, M., Di, C., Chu, L., Chen, B., Hu, Y., 2020a. Marine UAV-USV marsupial platform: system and recovery technic verification. Appl. Sci. 10 (5), 1583.
Zhang, Y., Edwards, C., Belmont, M., Li, G., 2022. Modeling and sliding-mode control for launch and recovery system in predictable sea states with feasibility check for collision avoidance. IEEE Trans. Control Syst. Technol. 30 (6), 2658–2671.
Zhang, Y., Edwards, C., Belmont, M., Li, G., 2023a. Robust model predictive control for constrained linear system based on a sliding mode disturbance observer. Automatica 154, 111101.
Zhang, Y., Stansby, P., Li, G., 2021. Non-causal linear optimal control with adaptive sliding mode observer for multi-body wave energy converters. IEEE Trans. Sustain. Energy 12 (1), 568–577.
Zhang, Y., Zeng, T., Li, G., 2020b. Robust excitation force estimation and prediction for wave energy converter m4 based on adaptive sliding-mode observer. IEEE Trans. Ind. Inf. 16 (2), 1163–1171.

Zhang, Y., Zhao, H., Li, G., Edwards, C., Belmont, M., 2023b. Robust nonlinear model predictive control of an autonomous launch and recovery system. IEEE Trans. Control Syst. Technol. 31 (5), 2082–2092.

Zhao, T., Sun, M., Wang, S., Han, G., Wang, H., Chen, H., Sun, Y., 2024. Dynamic analysis and robust control of ship-mounted crane with multi-cable anti-swing system. Ocean Eng. 291, 116376.